Geochemistry Geophysics Geosystems G3

Article
Volume 11, Number 6
29 June 2010
Q06017, doi:10.1029/2009GC002949
ISSN: 1525-2027

Published by AGU and the Geochemical Society

Pore fluid modeling approach to identify recent meltwater signals on the west Antarctic Peninsula

Zunli Lu and Rosalind E. M. Rickaby
Department of Earth Sciences, University of Oxford, Parks Road, Oxford OX1 3PR, UK (zunli.lu@earth.ox.ac.uk)

Julia Wellner
Department of Earth and Atmospheric Sciences, University of Houston, Houston, Texas 77204, USA

Bastian Georg
Department of Earth Sciences, University of Oxford, Parks Road, Oxford OX1 3PR, UK

Now at Worsfold Water Quality Center, Trent University, Peterborough, Ontario K9J 7B8, Canada

Norman Charnley
Department of Earth Sciences, University of Oxford, Parks Road, Oxford OX1 3PR, UK

John B. Anderson
Department of Earth Science, Rice University, Houston, Texas 77005, USA

Christian Hensen
Leibniz-Institut für Meereswissenschaften an der Universität Kiel (IFM-GEOMAR), D-24148 Kiel, Germany

[1] The sensitivity of sea level to melting from polar ice sheets and glaciers during recent natural and anthropogenic climate fluctuations is poorly constrained beyond the period of direct observation by satellite. We have investigated glacial meltwater events during the Anthropocene by adapting the pioneering approach of modeling trends in $\delta^{18}O$ in the pore waters of deep-sea cores, previously used to constrain the size of ice sheets during the Last Glacial Maximum. We show that during recent warm periods, meltwater from glacier retreat drains into the coastal fjords, leaving a signature of depleted $\delta^{18}O$ values and low Cl concentrations in the pore water profiles of rapidly accumulating sediments. Here we model such pore water profiles in a piston core to constrain the timing and magnitude of an ice sheet retreat event at Caley Glacier on the west Antarctic Peninsula, and the result is compared with local ice front movement. This approach of pore water modeling was then applied in another kasten core and tested by a series of sensitivity analyses. The results suggest that our approach may be applied in fjords of different sedimentary settings to reconstruct the glacier history and allow insight into the sensitivity of polar glaciers to abrupt warming events.

Components: 6800 words, 9 figures, 2 tables.

Keywords: pore water modeling; Antarctic Peninsula; meltwater; ice sheet; glaciers.

Index Terms: 1009 Geochemistry: Geochemical modeling (3610, 8410); 0720 Cryosphere: Glaciers; 0726 Cryosphere: Ice sheets.

Received 10 November 2009; **Revised** 26 April 2010; **Accepted** 5 May 2010; **Published** 29 June 2010.

Lu, Z., R. E. M. Rickaby, J. Wellner, B. Georg, N. Charnley, J. B. Anderson, and C. Hensen (2010), Pore fluid modeling approach to identify recent meltwater signals on the west Antarctic Peninsula, *Geochem. Geophys. Geosyst.*, *11*, Q06017, doi:10.1029/2009GC002949.

1. Introduction

[2] The stability of polar ice sheets in the face of recent climate warming is of great interest during our current phase of anthropogenic change. Any rapid decrease in ice volume due to recent climate warmings are of particular interest for predicting future sea level and feedbacks contributing to climate warming. Meltwater input may also have a significant impact on freshwater and nutrient supply to phytoplankton communities of the coastal regions [*Hendry and Rickaby*, 2008]. Currently, the mass balance of ice sheets on a large scale is best estimated using satellite data [*Rignot et al.*, 2005, 2008], but such direct observations only started in the early 1990s. Detailed records of migration in the ice sheet front derived from maps and aerial photographs can be compiled for the past ~60 years [*Cook et al.*, 2005]. However, the record of ice front advancing/retreating cannot be related directly to the changes of ice sheet volume, so reconstructing recent ice loss remains challenging for times prior to the satellite era. A tool to trace both the timing and magnitude of recent ice loss might provide a key to understand glacier response to short-term forcings such as the anthropogenic CO_2 input.

[3] Variation in polar ice volume can affect seawater salinity and stable oxygen isotope composition both in deep-sea basins and coastal regions like fjords, leaving global and local signatures at different time scales. An increase in $\delta^{18}O$ values and chloride concentrations associated with the last glacial maximum is preserved in pore waters of open ocean sediments [*Adkins and Schrag*, 2001; *Schrag and DePaolo*, 1993]. This feature was modeled to reconstruct the salinity and $\delta^{18}O$ content of the glacial ocean [*Adkins et al.*, 2002]. Compared to the global LGM signal in the deep ocean, pore waters in shallow fjord sediments should undergo a much stronger local influence of changing ice volume, as the fjords are small water masses close to the ice shelves. We have found a trend of isotopically light $\delta^{18}O$ values and decreased Cl concentrations in pore waters extracted from rapidly accumulating sediments at coastal West Antarctica, during U.S. Antarctica Program cruise NBP0703. In this paper, we model the meltwater signal (MWS) which could lead to such pore water chemistry changes. We are able to constrain the timing and flux of meltwater, in comparison with the movement of ice front and the flux of ice loss derived from satellite data in the Fleming and nearby glaciers. The applicability of the model in different sedimentary conditions is also investigated using sensitivity tests. Our results demonstrate that pore fluid modeling of the MWS is a useful method to extend our knowledge of modern glacier history beyond the last 20 years or so of satellite observations.

2. Study Area

[4] Samples used in this study were collected from six sites of the cruise NBP0703 to the Antarctic Peninsula region, which featured rapid sedimentation. Accumulation rates in thirteen sites of this cruise were determined by ^{210}Pb dating and range from 1.5 to 9.7 mm/yr (B. Hallet, unpublished data, 2010). The lithology in most cores is characterized by sandy to silty clay with occasional organic rich layers. Four of the six sites are located nearshore on the west Antarctic Peninsula between 64°S and 66°S (Figure 1 and Table A1). Recent warming across the peninsula has resulted in reducing ice sheet extent and the air temperature distribution indicates that the meteorological record of Faraday Vernadsky Station is representative for the four sites [*Vaughan and Doake*, 1996]. These records have been previously used to study ice sheet mass balance [*Vaughan*, 2006]. At the northern tip of the peninsula (Figure 1), JPC24 was cored in the deep Bransfield Basin at water depth of 1939 m and JPC2 was taken in a narrow region at the northern tip of the peninsula, where the temperature is ~3°C lower than all other sites [*Vaughan and Doake*, 1996].

3. Samples and Chemical Analyses

[5] Pore water samples were collected from 6 sites at the Antarctic Peninsula region. The size of the samples ranged from 1 to 15 ml. They were extracted from core sediments by centrifugation and filtered through a 0.2 μm filter immediately after the core recovery. The pore water was stored and transported in airtight containers for analysis at Department of Earth Sciences, University of Oxford.

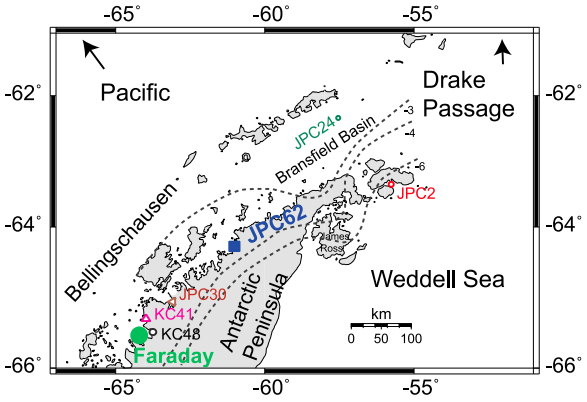

Figure 1. Site map of NBP0703. Dashed lines show mean annual temperature across the area [*Vaughan and Doake*, 1996]. All of the sites, except for JPC2 and JPC24, are in the same temperature zone with Faraday Vernadsky Station, and its summer temperature record is used in the model calibration.

[6] Oxygen isotope analyses were performed on a Thermo Finnigan Delta V Advantage isotope ratio mass spectrometer (IRMS) using a Gas Bench II peripheral unit equipped with a PAL autosampler. The analyses were calibrated against water standards from Iso-Analytical. Half a mL of each standard and sample were flushed for 6 min with 0.3% CO_2 in He, then left to equilibrate at 25°C for 18 h before being analyzed. Six repeating measurements on each samples typically reach a precision better than ±0.1‰.

[7] Chloride concentrations were analyzed on an automated Metrohm© IC 861 ion chromatograph using conductivity detection. Automated sample injection was accomplished via a fixed 20 μl injection loop. Anions were analyzed using a sequential suppression consisting of a MSM-II chemical suppressor followed by a Metrohm© 853-MCS CO2 suppressor. The analytical column used for anions was a Metrohm© Asupp5 (250 × 4 mm) using a mobile phase of 3.2 mM Na_2CO3/2.0 mM $NaHCO_3$/5% Acetone at a flow rate of 1.0 ml min^{-1}. The ion chromatography was calibrated against a series of standards with known concentration prior to each session. The repeatability (1RSD) is usually better than 1.5%, with no drift in baseline observed.

4. Meltwater Signal and End-Members of Water Masses

[8] The measured $\delta^{18}O$ compositions consistently decrease in the shallow part of the cores, reaching minimum values at depths between 1 and 3 m (Figure 2 and Table A2). JPC2 and JPC24 provide an exception and show little to no observable change. KC41, JPC30 and JPC62 (KC stands for kasten cores and JPC represent jumbo piston cores) recovered to more positive values at greater depth and show a peak of negative change. The peak is most pronounced at JPC 62 compared to other sites. The most depleted value (−1.44) was found at the bottom of the shortest core KC48. The possible loss of core top material is known for piston coring (JPC62 and JPC30), while kasten cores (KC41 and KC48) likely preserve the top better. However, the similar $\delta^{18}O$ signals in both kasten and piston cores implies that sediment loss for the top of JPC 62 is

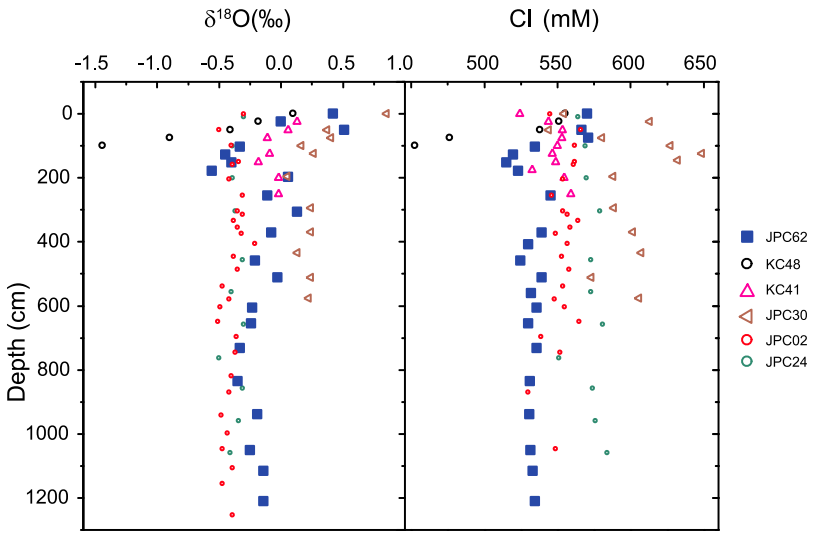

Figure 2. Oxygen isotope composition and chloride concentrations of the pore water samples.

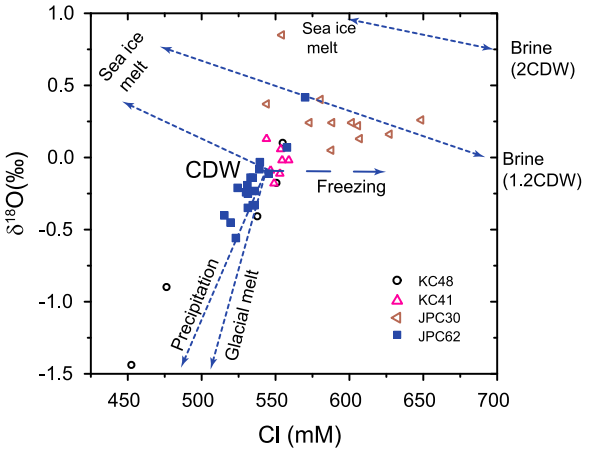

Figure 3. End-members and mixing processes affecting the pore water compositions. CDW stands for Circumpolar Deep Water, and brine (2CDW) stands for brines with 2 times of the salinity of CDW. The end-member compositions are CDW (−0.08‰, 544 mM), sea ice melt (+2‰, 110 mM), precipitation (−13‰, 0 mM), and glacial melt (−20‰, 0 mM) [*Meredith et al.*, 2008].

probably insignificant (Figure 2). The consistent $\delta^{18}O$ signals at similar depths in different sites also indicate that they were unlikely to be contaminated by freshwater during coring.

[9] The $\delta^{18}O$ decrease cannot be explained by diagenetic features such as clay transformation and gas hydrate dissociation, because they were observed at shallow depths (<5 m) above the sulfate methane transition, and at temperatures well below the window (60°C–120°C) for clay dehydration [*Bekins et al.*, 1995]. Since these sites are located in fjords, the negative peaks in measured pore water $\delta^{18}O$ compositions most likely reflect changes in the water isotope composition as a result of melt input influencing or mixing to the bottom of the entire fjord.

[10] The absence of a meltwater signal (MWS) at the two exceptional sites, JPC2 and JPC24, is most likely a result of their contrasting geographic locations. JPC 24 is located in the deep Bransfield Basin where any MWS is too dilute to detect. JPC 2 lies in a zone, ~3°C cooler than all other MWS sites (Figure 1). The highest summer temperature in the Faraday station and MWS sites is about 2°C. Any recent warming during the summer at JPC2 may still not cross the threshold of 0°C and result in any major glacier retreat.

[11] Chloride concentrations (Figure 2 and Table A2) display a MWS identical to the $\delta^{18}O$ profiles in sites JPC62 and KC48. No depth trend was found for the Cl concentrations in JPC2 and JPC24. However, the decoupling between the Cl and $\delta^{18}O$ is noticeable in JPC30, indicating the presence of different water masses. A crossplot of Cl versus $\delta^{18}O$ illustrates the mixing between main end-members and their influence at each individual site (Figure 3). The end-members include the Circumpolar Deep Water (CDW), sea ice melt, precipitation, glacial melt and brines with various salinities. Their chemical compositions are taken from a study of freshwater balance along the Antarctic Peninsula margin [*Meredith et al.*, 2008] and the mixing trends calculated accordingly are adequate to explain the measured values in our sites. The pore waters with positive $\delta^{18}O$ values are mixtures of three end-members including CDW, sea ice melts and brines concentrated to different degrees by seawater freezing.

[12] The strong MWS in JPC62, KC41 and KC48 reflect the mixing dominantly between the CDW and glacial melts/meteoric water, with very minor influence of the sea ice melt and brines (Figure 3). No lithological changes indicate that the MWS in all of these three sites are related to freshwater input within sediment column. Such sources, if responsible for the MWS, must be located at the depth with minimum $\delta^{18}O$ value (~1–2 m, Figure 2). Within this interval, JPC62 contains homogeneous silty clay and KC41 contains sandy silty mud with few clay rich layers. KC48 has relatively low sample recovery and did not reach deep enough to catch the minima in pore water profiles as in JPC62 and KC41. Therefore the $\delta^{18}O$ and Cl profiles of JPC62 and KC41 were chosen as the best candidates for modeling the meltwater input.

5. Model Setup

[13] A solute transport model was written in Mathematica for simulating the depth profiles of $\delta^{18}O$ and Cl compositions. Partial differential equations were set up following the established method [*Berner*, 1980; *Boudreau*, 1997], and the same as the method used for LGM $\delta^{18}O$ and salinity modeling [*Adkins and Schrag*, 2003; *Adkins et al.*, 2002].

$$\phi\frac{\partial C}{\partial t}=\frac{\partial}{\partial z}\left(\phi\cdot D\cdot\frac{\partial C}{\partial z}\right)-\frac{\partial}{\partial z}(\phi\cdot v\cdot C)+\phi\cdot R \qquad (1)$$

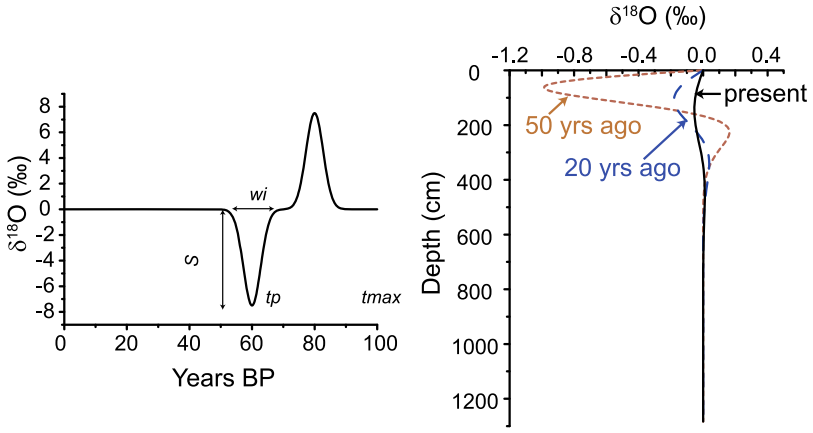

Figure 4. Pore water evolution/relaxation from 50 years ago to present, after a hypothetical perturbation of bottom water compositions (60–80 years B.P.).

where z is depth, t is time, φ is porosity, D is the diffusion coefficients, C is the concentration of dissolved species in pore water, v is the advection velocity of solutes and R is the reaction rates. The model considers the decrease in porosity with sediment depth, steady state compaction, advective transport of solutes, and molecular diffusion of dissolved species. Details about how these processes are modeled, including the constitutive equations, can be found in [*Wallmann et al.,* 2008, and references therein]. The reaction term (R) is not considered in this model.

[14] Previous studies suggested that results of such model are sensitive to the diffusion coefficients [*Adkins and Schrag*, 2003; *Schrag and DePaolo*, 1993]. In these studies, the experimentally determined D^o values in seawater [*Li and Gregory*, 1974] were first corrected (D_{corr}) by temperature, porosity and tortuosity and then the D_{corr} was adjusted to obtain the effective diffusion coefficients (D_{eff}). The D_{eff} used to produce final results was chosen by adjusting k values (0.3–1 different for each site) with advection rates to obtain the best fit between the measured data and modeled profiles. Because the MWS modeled here is a much shallower feature (1–2 m) compared with the signature of the LGM (20–50 m), the processes responsible for the difference between D_{eff} and D_{corr}, like electrical gradients and bioturbation [*Adkins and Schrag*, 2003], should have much less cumulative influence in our sites. The same set of D_{corr} values [*Boudreau*, 1997], instead of D_{eff}, are used for the sites modeled here and the sensitivity of modeling results to the D_{corr} is discussed later.

[15] Top and bottom of the core are represented by the upper and lower boundary conditions, respectively. The lower boundary uses a Dirichlet boundary condition when calculating the temporal evolution of the model. Variations in the bottom water composition (upper boundary) due to meltwater or brine injection are simulated using the following form:

$$\delta^{18}O[t] = \delta^{18}O_{t\,\max} - S_1 \cdot e^{\left[(tp1-t)^2/wi_1\right]} - S_2 \cdot e^{\left[(tp2-t)^2/wi_2\right]} \ldots . \quad (2)$$

where $\delta^{18}O$ [t] stands for the bottom water composition at time t, $t$max for the length of modeled time period, $\delta^{18}O_{t\max}$ for the composition at the end of the model run, S as a scaling factor to adjust the variation in the composition during each melting event, tp to adjust the time when the composition reaches the largest change during each melting event, wi to change the duration of each melting event (Figure 4, for example).

[16] Finite difference techniques (the method-of-lines code) are used to solve the model [*Boudreau*, 1996; *Hensen and Wallmann*, 2005; *Lu et al.*, 2008; *Wallmann et al.*, 2008]. The partial differential equations defining each species in the model are converted into a large number of ordinary differential equations (ODE) for the temporal variation of concentration at each depth interval. The ODE system is set up on an uneven grid with increasing resolution toward the core top. It is solved using the NDSolve object of Mathematica Version 5.

[17] A preliminary model run, assuming some hypothetical changes in the bottom water composition, was first used to roughly simulate the observed pore water trend and test the pore water

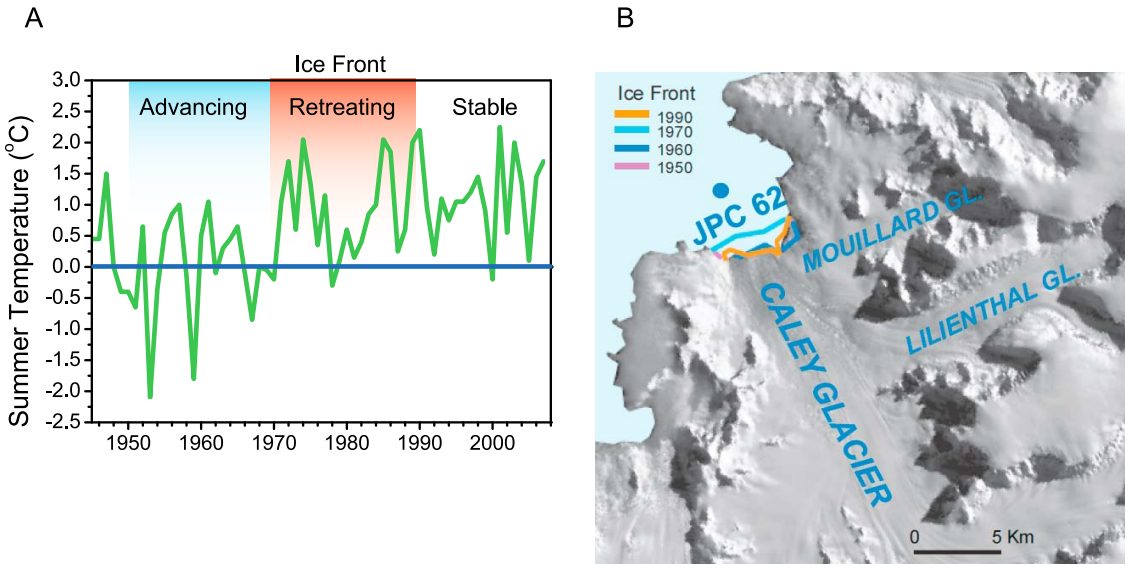

Figure 5. (a) The summer temperature record from Faraday Vernadsky and (b) local ice front movement since 1950.

relaxation (Figure 4). During the model run of 100 years, the upper boundary was forced to change in opposite directions in two separate events, negative $\delta^{18}O$ around 60 years B.P. and positive $\delta^{18}O$ for 80 years B.P. Immediately after these two events (50 years B.P.), a strong shift toward negative values was found between 0 and 100 cm below seafloor and a positive shift at around 200 cm in the depth profile, similar to the trends observed in the cores from the Antarctic Peninsula studied here. This relaxation test suggests that the relatively recent event is much better preserved in the pore water profile, even though the previous event has the same magnitude and duration. The MWS in pore water profiles gradually moves to deeper depths over time and its signal weakens. Furthermore, this relaxation test suggests that the observed MWS is a short-lived feature which was produced by a recent meltwater pulse and will be smoothed out by diffusion after roughly 50–100 years depending on the scale of the pulse.

6. Modeling the MWS

[18] JPC62 has pore water profiles with the most clearly defined MWS and only show minor influence of the brines and sea ice (Figure 3), making it the best candidate for the model calibration. We first calibrate the model to determine the timing of the event at JPC62, using upper boundary functions linked to the instrumental temperature record from Faraday Vernadsky Station. We then estimate the flux and total volume of meltwater during the event. Finally, we also model KC41 and use the results of sensitivity tests to show the applicability of the model in different sedimentary conditions. Overall, the MWS shape is sensitive to the timing, duration of the meltwater event and the bottom water composition, but insensitive to sedimentary settings. The model provides relatively good constraints on the timing, while multiple solutions can be obtained for the bottom water composition without independent constraint on sea ice and brine dynamics.

6.1. Calibrating the Timing of Meltwater Injection

[19] Both the temperature record and the ice front movement are useful for constraining the timing of melt events at JPC62. The summer temperatures recorded at Faraday Vernadsky Station extend back to 1945 (Figure 5a), showing relatively colder summer before 1970 and several periods of warming with similar magnitude after 1970. A compilation of aerial photos of the Antarctic Peninsula yield a record for the movement of the ice front (Figure 5b) [*Ferrigno et al.*, 2006]. JPC62 is located in the Brialmont Cove of Hughes Fjord, a drainage fjord of Cayley Glacier, Mouillard Glacier, and Lilienthal Glacier. The local ice front advanced between the 1950 to 1970 and then retreated between the 1970 to 1990, coinciding with the cold and warm period before 1990. However, the ice front appears to have remained stable since 1990, rather unresponsive to the most recent warming.

[20] We constructed three upper boundary functions (based on temperature) to represent three scenarios of bottom water conditions, with an increasing number of factors which have a nonlinear relationship to the temperature: (1) bottom water compositional changes linearly depending on summer temperature, (2) incorporating the ice front movement into upper boundary conditions, and (3) bottom water composition nonlinearly dependent on summer temperature during brine formation and taking into account sea ice melt. We assume that glacial melts are triggered by summer temperatures climbing above 0°C, causing a decrease in bottom water chlorinity and $\delta^{18}O$ values. On the other hand, seawater freezing (brine formation) occurs at temperatures below 0°C and causes increase in the chlorinity but negligible changes in $\delta^{18}O$. The upper boundary functions are, therefore, constructed according to these compositional changes, with the duration of each event (melting or freezing) fixed based on the temperature fluctuation (Figure 6).

[21] For scenario 1, the changes in bottom water chlorinity and $\delta^{18}O$ were scaled to match the changes in temperature in the entire modeled period (Figure 6), except for holding $\delta^{18}O$ values unchanged during seawater freezing. Minima in the modeled MWS of Cl and $\delta^{18}O$ are shallower than those in the measured profiles. It suggests that the latest melting event adopted in this scenario is younger than the event responsible for the MWS seen in our cores. Alternatively, the values of diffusion coefficient used in the model, if too small, could potentially delay the downward propagation of bottom water changes in the model and result in shallow MWS. However, the effective diffusion coefficients estimated for DSDP/ODP sites (e.g., 208 cm^2/yr for ^{18}O at core top [*Schrag and DePaolo*, 1993]) were all lower than the values used in this model (273 cm^2/yr for ^{18}O at core top, see section 5). So the shallow MWS should not be an artifact of the modeling procedure related to underestimated diffusion coefficients. It is more likely related to recent decreases in fresh water input, coinciding with the observed stabilization of ice front since 1990.

[22] Scenario 2 was designed to test the possibility of limited fresh water input between 1990 and 2005 by disabling the recent melting events (Figure 6). The modeling results are significantly improved for both Cl and $\delta^{18}O$ as indicated by the R values. There are also good matches between the depth of modeled and measured MWS center, suggesting that the two warming periods around 1975 and 1985 are responsible for the observed MWS in JPC62. Furthermore, if we consider the possibility of a ~0.5–1 m sediment loss during coring, in order to produce a MWS deeper than the measured profile at JPC62, the melting would have to happen >10 years earlier. Such a melt input is inconsistent with the best knowledge of the ice front record.

[23] In scenario 2, the modeled $\delta^{18}O$ values are lower than the measured values at 200–300 cm and the Cl minimum is also underestimated even with the bottom water forced to pure fresh water at the strongest melt input (Figure 6). Both of these misfits are probably caused by the nonlinear correlation between the bottom water composition and summer temperature, related to the sea ice and brines. We consider these nonlinear factors in scenario 3. The positive $\delta^{18}O$ values around 200–300 cm (right beneath the MWS) suggest that sea ice melt, the only end-member with positive $\delta^{18}O$ values (Figure 3), almost certainly was injected before the main glacial melt in the 1970s. In scenario 3, we model the influence of sea ice melt by forcing the $\delta^{18}O$ to positive values (<+3‰) in the upper boundary during warm periods before 1970 (Figure 6). Such an upper boundary condition further improved the model results for the $\delta^{18}O$ profile (Figure 6). The underestimated Cl minimum in the modeled downcore trend of scenario 2 is due to overshooting of brine formation (Cl > 544 mM) in the upper boundary before 1970, which counterbalanced part of the glacial melt signal. Because the brine generation is dominantly controlled by the winter temperature, not the summer temperature, the Cl increase during brine formation was then allowed to be nonlinear with the summer temperature and was gradually reduced to find the best model result. The effect of brine in scenario 3 is about one third of that in scenario 2 and such an upper boundary well reproduced the MWS in the Cl profile.

[24] To summarize, the observed MWS was mainly produced by the glacial melt between 1970 and 1990, the first prolonged warming period since 1945. Any significant melting after 1990 would result in a MWS shallower than those in the measured pore water profiles. These modeling results are consistent with the ice front record. The influence of sea ice melt and brine formation can be considered in the model. They further improve the model fit, but do not change the calibration of the timing for the major glacial melting event and they are not central to the aim of this study.

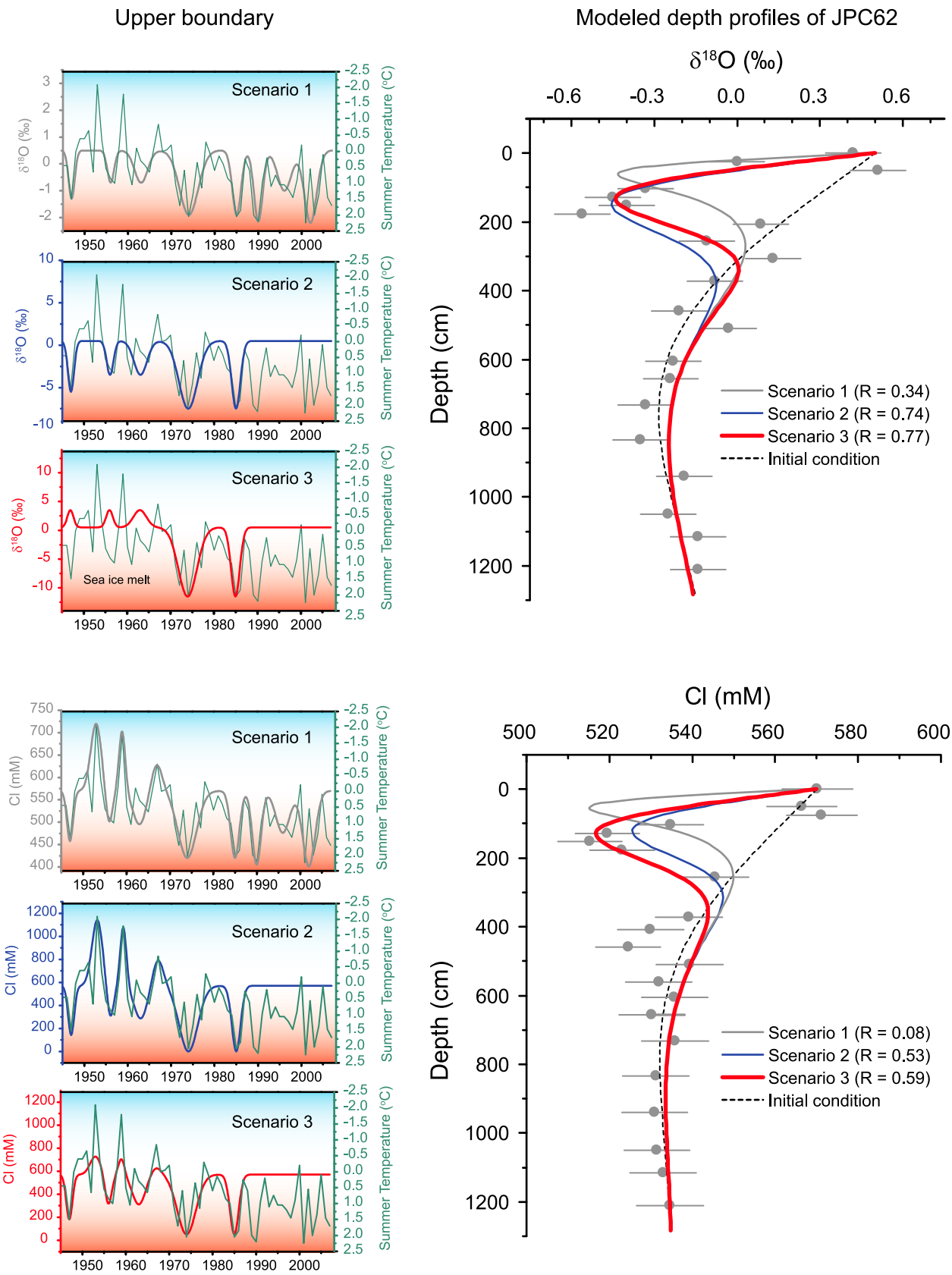

Figure 6. The upper boundary conditions used for three scenarios and the model results of JPC62. Temperatures are plotted on reverse scale.

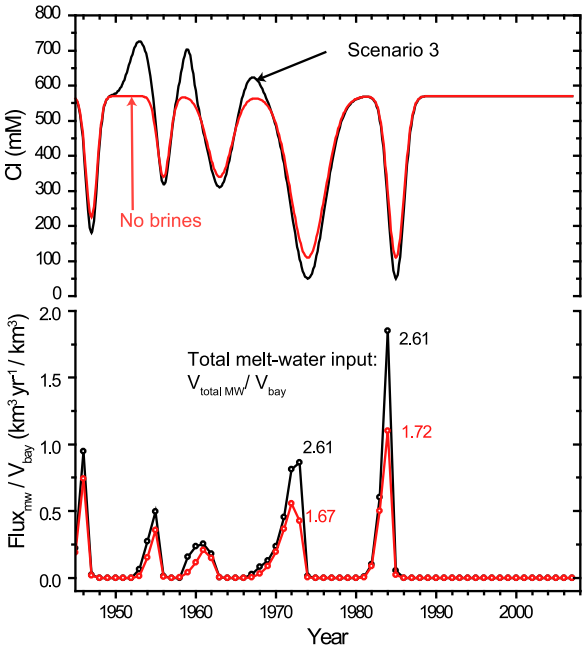

Figure 7. (bottom) Meltwater flux of JPC62 calculated from (top) the Cl upper boundary functions. Black curves are for scenario 3, and red curves are for the upper boundary excluding the brine generation.

6.2. Approximation of the Meltwater Input Using the Cl Profile

[25] Although both the $\delta^{18}O$ and Cl profiles provide equally good constraints on the timing of the melt event, the $\delta^{18}O$ profile alone cannot be used to calculate the volume of meltwater input. The MWS of JPC62 is mainly caused by a mixture of glacial melt (−20‰) and precipitation (−13‰) (Figure 3). Because of the different $\delta^{18}O$ values in these end-members, the precision of the volume estimate would suffer from lack of information about their relative contributions. On the other hand, both glacial melt and precipitation contains negligible Cl, compared to seawater and sea ice, making Cl a more sensitive proxy for the volume of meltwater input.

[26] A mass balance calculation can be used to estimate the flux and total meltwater volume using the Cl upper boundary function. The mass balance of Cl during the mixing between the meltwater and fjord water can be considered stepwise:

$$Cl[t] \cdot V_{bay} + 0 \cdot Flux_{MW} = Cl[t+1] \cdot \left(V_{bay} + Flux_{MW}\right) \quad (3)$$

$Cl[t]$, $Cl[t+1]$ are the Cl concentration of bottom water at year t and t + 1. V_{bay} is the volume of the fjord. $Flux_{MW}$ is the volume of meltwater added each year. The ratio of $Flux_{MW}/V_{bay}$ can be derived for each year and the ratio between cumulative meltwater volume and the fjord volume ($V_{total\ MW}/V_{bay}$) was also calculated (Figure 7). The chlorinity at the strongest melt input (around 1975 and 1985) was close to that of fresh water in scenario 3 (black curves, Figure 7). Such an upper boundary is used to derive a maximum estimate for meltwater volume. A minimum estimate for meltwater volume can be calculated by disabling brine formation before 1970 (red curves, Figure 7). Both upper boundaries produce identical modeled Cl depth profiles. The total volumes of meltwater are very similar to each other during two glacial melt events in the 1970s and 1980s, about twice the size of the fjord. The shorter melting event in the 1980s has higher annual meltwater flux at the time of strongest melt input. Assuming the volume of the fjord to be 4–5 km^3 (Figure 5b), the highest annual flux (at 1984) calculated here corresponds to 8.2–10.3 km^3/yr of ice, comparable to the recent (1995–2004) discharge rate of Wordie Ice Shelf (6.8 km^3/yr), further south of the west Antarctic Peninsula [*Rignot et al.*, 2005]. Our flux calculation falls into a reasonable range compared to the satellite data, but we will discuss the uncertainties of this approach in section 6.3.

6.3. Potential Applications, Limiting Factors, and Caveats

[27] Profiles of KC41 are also modeled (Figure 8) to demonstrate that the approach can be applied to different sites. Core KC41 was taken close to Faraday station, but even forcing the upper boundary completely by temperature (like scenario 1 of JPC62) still produced a MWS shallower than that in the measured data (better represented by the Cl profiles, gray lines in Figure 8). Cl concentrations decrease toward the top of KC41, likely indicating a developing MWS from the most recent period. A small freshwater input starting at 2005 (marked by gray bars) is added to the upper boundary forcing similar to scenario 3 in JPC62 and such a bottom water composition is sufficient to model the measured profiles. Comparing the $\delta^{18}O$ profile with the Cl profile in KC41, data resolution and precision appear to be important factors influencing the uncertainty of model calibration. High-resolution and high-precision pore

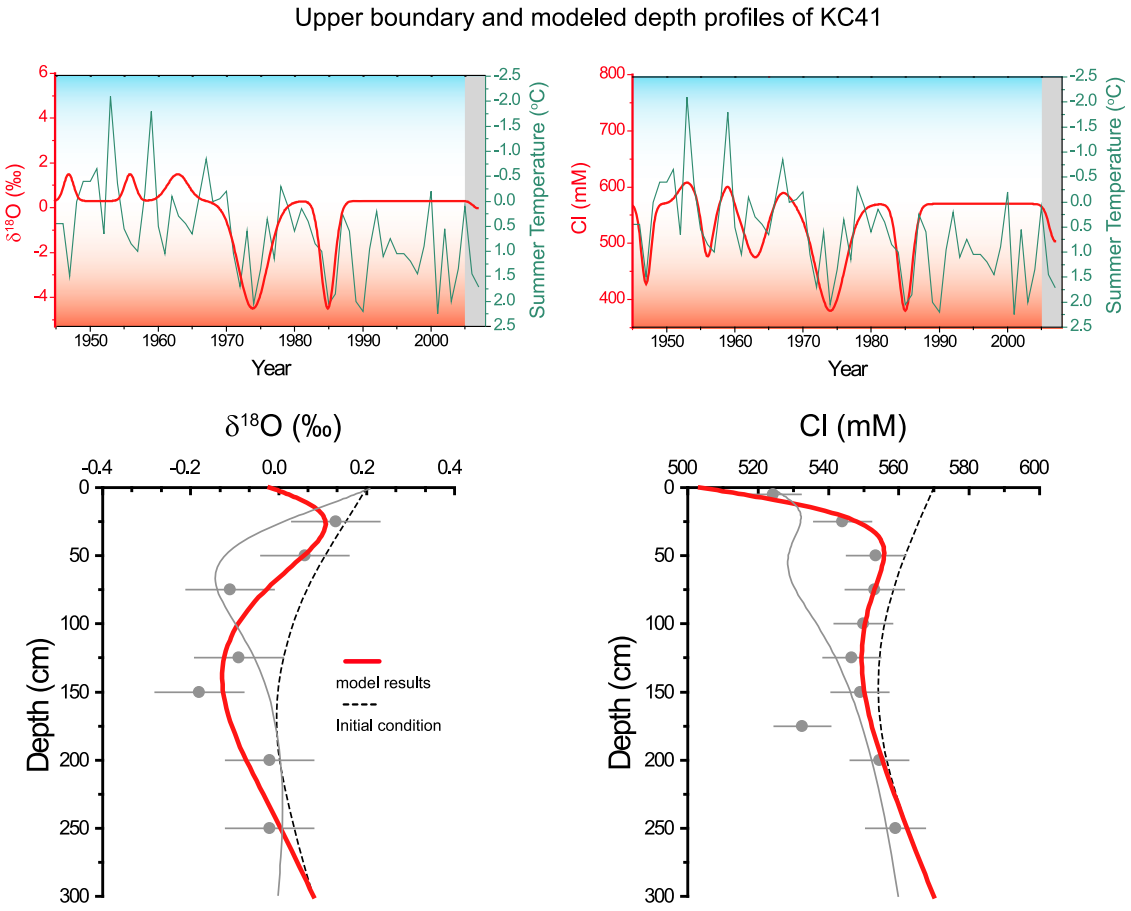

Figure 8. Meltwater input since 2005 is added to the upper boundaries of scenario 3 for JPC62. Such upper boundaries are sufficient to model the profiles in site KC41 (red lines). Gray lines are the modeling results obtained with upper boundary linearly forced by temperature, similar to scenario 1 for JPC62.

water measurements particularly in the upper 5 m of the core can significantly facilitate the model calibration of the recent MWS. The location of the cores is also important for application of this approach. Since water depth, distance to glacier and sea ice play a role in the bottom water composition, nearshore sites in shallow fjords without obvious influence of sea ice are more likely to record the MWS better, although the brine signal (e.g., high Cl concentrations in JPC30) may also be modeled to constrain sea ice dynamics.

[28] Figure 4 demonstrates how the meltwater peak would broaden and deepen in older events, indicating that the model could be calibrated to simulate major melting input of at least 40–50 years ago. The pore water modeling approach provides an opportunity to reconstruct ice sheet melting for time slices before satellite data are available. A series of sensitivity analyses of fluid rate, porosity sedimentation rate and diffusivity are applied to the Cl profile of JPC62 (Figure 9) to show the potential of applying this pore water modeling approach in different sedimentary environments. The MWS at such shallow depths are dominated by the bottom water conditions and relatively insensitive to the difference in sedimentary settings. Varying flow rates between 0 and 0.1 cm/yr, the typical range of compaction driven advection at nonseep sites, did not produce any visible changes in the model results (Figure 9a). It is not surprising because advection within ~20–30 years at such rates probably cannot move the MWS beyond a few cm in the core. Changes in the porosity also affect the MWS in only a very small way (Figure 9b). With the same bottom water boundary condition, higher sedimentation rate helps to preserve the MWS, i.e., lower values at the Cl minimum, and the MWS was not shifted vertically in the profile (Figure 9c). Similar to flow rates, the very recent MWS

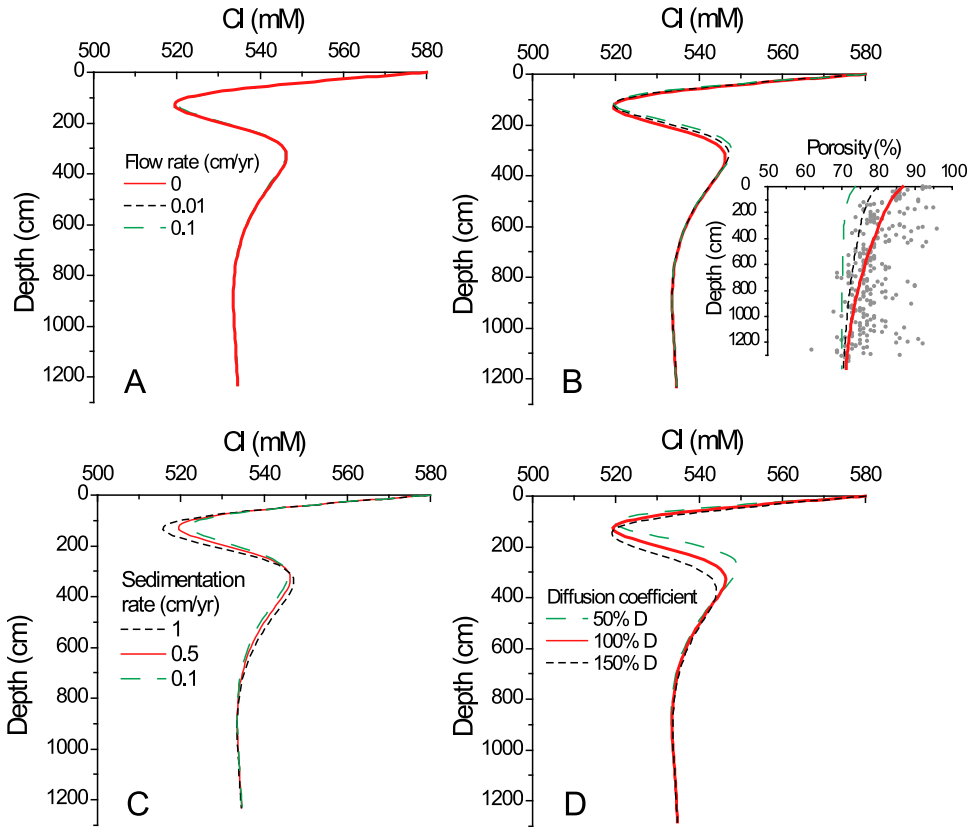

Figure 9. Sensitivity tests for various flow and sedimentation conditions. These parameters were not measured for JPC62, and the range of values were taken for the typical settings around the Antarctic Peninsula. The red lines represent the parameterization actually adopted in the model runs in Figures 4 and 6–8. The porosity data are from JPC2 [*Michalchuk et al.*, 2009].

(20 years) modeled here should not be significantly affected by sedimentation rates found in this area (~1–10 mm/yr). In contrast, the LGM model of a much older signal (20 kyr) should be more sensitive to the sedimentation regime. When the diffusivity was varied by ±50% (149–288 cm^2/yr for Cl at core top), the center of the MWS shifted slightly but the width of MWS responded more strongly (Figure 9d). In order to check the influence of effective diffusivity, nonelectrical species like silicic acid and boric acid might be useful to measure and incorporate into the model in a future study, although large changes in diffusivity are not likely in shallow pore waters. Based on these sensitivity analyses, the modeling approach presented here has potential application to fjords of various sedimentary settings to study recent glacier history.

[29] Pore water profiles record changes in bottom water composition for periods of centennial scale. However, bottom water composition may decouple from glacial mass balance due to processes like sea ice dynamics and water stratification in the fjord, which cannot be addressed satisfactorily in this study with the available information. In both JPC62 and KC41, warming in the 90s did not cause significant freshening of the bottom water (Figures 6 and 8). In addition to the possibility of decreased glacier melting during that period, alternative explanations might include the possibility that strong stratification prevented meltwater reaching the bottom of the fjord. The flux (Figure 7) derived from the upper boundary only provides a first-order approximation to the meltwater volume and the uncertainty in this type of estimation clearly needs to be further tested in fjords where glacial freshwater input has been derived independently by other methods. Furthermore, summer temperatures are chosen to constrain the upper boundary in the model, whereas local glacial mass balance might be

affected by warming in other seasons [*Stammerjohn et al.*, 2008], atmospheric positive degree days [*Vaughan*, 2006], and melting of the marine terminus by warm water masses [*Martinson et al.*, 2008]. The upper boundary function can be easily modified if detailed time series are available for these potential controlling factors.

7. Conclusions

[30] The history of glacier retreat and ice loss in the polar regions due to climate warming is critical in predicting sea level changes and understanding sensitivity of polar ice to short-term warming. Meltwater that drained into glacier fjords leaves a signature in pore water chemical profiles. The meltwater signals of depleted $\delta^{18}O$ values and low Cl concentrations found at the west Antarctic Peninsula have been modeled to constrain the timing and volume of meltwater input. Meltwater injection between 1970 and 1990 produces the best fit to the measured $\delta^{18}O$ profile, consistent with the ice front retreating at the same time. The Cl upper boundary was then used to calculate ice flux during such an event and yielded maximum flux of about 8.2–10.3 km^3/yr, comparable to the published value at a nearby fjord. This kind of flux estimate can be achieved by the model to at least ~1940. Because the meltwater signals are controlled by bottom water chemistry and are insensitive to different sedimentary conditions, this pore fluid model might be applied in various fjords to derive a record of major glacial melting events before the satellite era.

Appendix A

[31] Table A1 provides site locations. Table A2 gives Cl concentrations and oxygen isotope compositions of pore waters.

Table A1. Site Locations

Sites	Longitude	Latitude
JPC2	−55°53′	−63°21′
JPC24	−57°39′	−62°16′
JPC30	−63°06′	−65°03′
KC41	−65°21′	−65°21′
KC48	−65°21′	−65°21′
JPC62	−60°60′	−64°17′

Table A2. The $\delta^{18}O$ and Cl Concentrations of the Pore Water Samples

Depth (cm)	Cl (mM)	$\delta^{18}O$ (‰)
	JPC62	
0	570	0.42
50	566	0.00
75	571	0.51
103	535	−0.33
128	520	−0.45
153	515	−0.40
178	523	−0.56
255	545	−0.11
372	539	
409	530	0.13
459	525	−0.08
511	539	−0.21
561	532	−0.03
606	536	−0.23
656	530	−0.24
733	536	−0.33
835	531	−0.35
939	531	−0.19
1051	531	−0.25
1116	533	−0.14
1210	535	−0.14
	KC41	
0	524	
25	544	0.13
50	553	0.06
75	553	−0.11
100	550	
125	547	−0.09
150	549	−0.18
175	533	
200	554	−0.02
250	559	−0.02
	KC48	
0	555	0.10
25	551	−0.18
50	538	−0.41
75	477	−0.90
100	453	−1.44
	JPC30	
0	554	0.85
25	613	
50	544	0.37
75	580	0.40
100	627	0.16
125	648	0.26
146	632	
196	588	0.05
294	588	0.24
369	601	0.24
434	607	0.13
512	573	0.24
577	606	0.22
	JPC24	
10	564	−0.30
101	569	−0.39
202	570	−0.39

Table A2. (continued)

Depth (cm)	Cl (mM)	$\delta^{18}O$ (‰)
305	579	−0.37
457	573	−0.31
557	573	−0.40
659	581	−0.30
763	551	−0.50
859	574	−0.31
960	576	−0.34
1060	584	−0.41
	JPC2	
1	545	−0.30
50	566	−0.50
100	562	−0.40
150	562	−0.34
160	561	−0.39
205	554	−0.42
255	546	−0.31
305	554	−0.35
315	557	−0.31
335	564	−0.38
355	559	−0.35
375	549	−0.32
407	557	−0.21
447	553	−0.38
487	558	−0.35
539	554	−0.47
579	548	−0.42
605	555	−0.49
650	565	−0.51
697	539	−0.36
747	552	−0.37
820		−0.40
870	530	−0.42
942		−0.48
998		−0.43
1048	549	−0.47
1107		−0.39
1157	344	−0.47
1254		−0.39
1414	549	−0.41
1464	555	−0.32
1565	563	−0.27
1661	556	−0.26
1937	533	−0.40
1994		−0.47

Acknowledgments

[32] We are grateful to the scientific party and crew members of NBP0703. We thank Bernie Boudreau and John Higgins for discussing the idea and helping the model setup. The manuscript benefited greatly from thorough and constructive reviews by Robert McKay, Matthew O'Regan, an anonymous reviewer and comments by Editor Vincent Salters. This work is supported by Natural Environment Research Council (NERC award NE/E014801/1 to R. E. M. Rickaby).

References

Adkins, J. F., and D. P. Schrag (2001), Pore fluid constraints on deep ocean temperature and salinity during the Last Glacial Maximum, *Geophys. Res. Lett.*, *28*(5), 771–774, doi:10.1029/2000GL011597.

Adkins, J. F., and D. P. Schrag (2003), Reconstructing Last Glacial Maximum bottom water salinities from deep-sea sediment pore fluid profiles, *Earth Planet. Sci. Lett.*, *216*(1–2), 109–123, doi:10.1016/S0012-821X(03)00502-8.

Adkins, J. F., K. McIntyre, and D. P Schrag (2002), The salinity, temperature, and $\delta^{18}O$ of the glacial deep ocean, *Science*, *298*(5599), 1769–1773, doi:10.1126/science.1076252.

Bekins, B. A., A. M. McCaffrey, and S. J. Dreiss (1995), Episodic and constant flow models for the origin of low-chloride waters in a modern accretionary complex, *Water Resour. Res.*, *31*(12), 3205–3215, doi:10.1029/95WR02569.

Berner, R. A. (1980), *Early Diagenesis: A Theoretical Approach*, Princeton Univ. Press, Princeton, N. J.

Boudreau, B. P. (1996), A method-of-lines code for carbon and nutrient diagenesis in aquatic sediments, *Comput. Geosci.*, *22*(5), 479–496.

Boudreau, B. P. (1997), *Diagenetic Models and Their Implementation*, Springer, Berlin.

Cook, A. J., A. J. Fox, D. G. Vaughan, and J. G. Ferrigno (2005), Retreating glacier fronts on the Antarctic Peninsula over the past half-century, *Science*, *308*(5721), 541–544, doi:10.1126/science.1104235.

Ferrigno, J. G., A. J. Cook, K. M. Foley, R. S. Williams Jr., C. Swithinbank, A. J. Fox, J. W. Thomson, and J. Sievers (2006), Coastal-change and glaciological map of the Trinity Peninsula area and South Shetland Islands, Antarctica: 1843–2001, *U.S. Geol. Surv. Geol. Invest. Ser. Map, I-2600-A*.

Hendry, K. R., and R. E. M. Rickaby (2008), Opal (Zn/Si) ratios as a nearshore geochemical proxy in coastal Antarctica, *Paleoceanography*, *23*, PA2218, doi:10.1029/2007PA001576.

Hensen, C., and K. Wallmann (2005), Methane formation at Costa Rica continental margin—Constraints for gas hydrate inventories and cross-decollement fluid flow, *Earth Planet. Sci. Lett.*, *236*(1–2), 41–60, doi:10.1016/j.epsl.2005.06.007.

Li, Y.-H., and S. Gregory (1974), Diffusion of ions in seawater and in deep-sea sediments, *Geochim. Cosmochim. Acta*, *38*(5), 703–714, doi:10.1016/0016-7037(74)90145-8.

Lu, Z., C. Hensen, U. Fehn, and K. Wallmann (2008), Halogen and ^{129}I systematics in gas hydrate fields at the northern Cascadia margin (IODP Expedition 311): Insights from numerical modeling, *Geochem. Geophys. Geosyst.*, *9*, Q10006, doi:10.1029/2008GC002156.

Martinson, D. G., S. E. Stammerjohn, R. A. Iannuzzi, R. C. Smith, and M. Vernet (2008), Western Antarctic Peninsula physical oceanography and spatio-temporal variability, *Deep Sea Res., Part II*, *55*(18–19), 1964–1987, doi:10.1016/j.dsr2.2008.04.038.

Meredith, M. P., M. A. Brandon, M. I. Wallace, A. Clarke, M. J. Leng, I. A. Renfrew, N. P. M. van Lipzig, and J. C. King (2008), Variability in the freshwater balance of northern Marguerite Bay, Antarctic Peninsula: Results from $\delta^{18}O$, *Deep Sea Res., Part II*, *55*(3–4), 309–322, doi:10.1016/j.dsr2.2007.11.005.

Michalchuk, B. R., J. B. Anderson, J. S. Wellner, P. L. Manley, W. Majewski, and S. Bohaty (2009), Holocene climate and

glacial history of the northeastern Antarctic Peninsula: The marine sedimentary record from a long SHALDRIL core, *Quat. Sci. Rev.*, *28*(27–28), 3049–3065, doi:10.1016/j.quascirev.2009.08.012.

Rignot, E., G. Casassa, S. Gogineni, P. Kanagaratnam, W. Krabill, H. Pritchard, A. Rivera, R. Thomas, J. Turner, and D. Vaughan (2005), Recent ice loss from the Fleming and other glaciers, Wordie Bay, West Antarctic Peninsula, *Geophys. Res. Lett.*, *32*, L07502, doi:10.1029/2004GL021947.

Rignot, E., J. L. Bamber, M. R. van den Broeke, C. Davis, Y. Li, W. J. van de Berg, and E. van Meijgaard (2008), Recent Antarctic ice mass loss from radar interferometry and regional climate modelling, *Nat. Geosci.*, *1*(2), 106–110, doi:10.1038/ngeo102.

Schrag, D. P., and D. J. DePaolo (1993), Determination of $\delta^{18}O$ of seawater in the deep ocean during the Last Glacial Maximum, *Paleoceanography*, *8*(1), 1–6, doi:10.1029/92PA02796.

Stammerjohn, S. E., D. G. Martinson, R. C. Smith, and R. A. Iannuzzi (2008), Sea ice in the western Antarctic Peninsula region: Spatio-temporal variability from ecological and climate change perspectives, *Deep Sea Res., Part II*, *55*(18–19), 2041–2058, doi:10.1016/j.dsr2.2008.04.026.

Vaughan, D. G. (2006), Recent trends in melting conditions on the Antarctic Peninsula and their implications for ice-sheet mass balance and sea level, *Arct. Antarct. Alp. Res.*, *38*(1), 147–152.

Vaughan, D. G., and C. S. M. Doake (1996), Recent atmospheric warming and retreat of ice shelves on the Antarctic Peninsula, *Nature*, *379*(6563), 328–331, doi:10.1038/379328a0.

Wallmann, K., G. Aloisi, M. Haeckel, P. Tishchenko, G. Pavlova, J. Greinert, S. Kutterolf, and A. Eisenhauer (2008), Silicate weathering in anoxic marine sediments, *Geochim. Cosmochim. Acta*, *72*(12), 2895–2918, doi:10.1016/j.gca.2008.03.026.